

## Fission fragment angular distributions in pre-actinide nuclei

Tathagata Banerjee,<sup>1,\*</sup> S. Nath,<sup>1</sup> A. Jhingan,<sup>1</sup> Gurpreet Kaur,<sup>2</sup> R. Dubey,<sup>1</sup> Abhishek Yadav,<sup>1</sup> P. V. Laveen,<sup>3</sup> A. Shamlath,<sup>3</sup> M. Shareef,<sup>3</sup> J. Gehlot,<sup>1</sup> N. Saneesh,<sup>1</sup> E. Prasad,<sup>3,†</sup> P. Sugathan,<sup>1</sup> and Santanu Pal<sup>4,‡</sup>

<sup>1</sup>*Nuclear Physics Group, Inter University Accelerator Centre, Aruna Asaf Ali Marg, Post Box 10502, New Delhi 110067, India*

<sup>2</sup>*Department of Physics, Panjab University, Chandigarh 160014, India*

<sup>3</sup>*Department of Physics, School of Mathematical and Physical Sciences, Central University of Kerala, Kasaragod 671314, India*

<sup>4</sup>*CS-6/1, Golf Green, Kolkata 700095, India*

(Received 22 July 2016; published 13 October 2016)

**Background:** Complete fusion of two nuclei leading to formation of a heavy compound nucleus (CN) is known to be hindered by various fission-like processes, in which the composite system reseparates after capture of the target and the projectile inside the potential barrier. As a consequence of these non-CN fission (NCNF) processes, fusion probability ( $P_{\text{CN}}$ ) starts deviating from unity. Despite substantial progress in understanding, the onset and the experimental signatures of NCNF and the degree of its influence on fusion have not yet been unambiguously identified.

**Purpose:** This work aims to investigate the presence of NCNF, if any, in pre-actinide nuclei by systematic study of fission angular anisotropies and fission cross sections ( $\sigma_{\text{fis}}$ ) in a number of nuclear reactions carried out at and above the Coulomb barrier ( $V_{\text{B}}$ ).

**Method:** Fission fragment angular distributions were measured for six  $^{28}\text{Si}$ -induced reactions involving isotopically enriched targets of  $^{169}\text{Tm}$ ,  $^{176}\text{Yb}$ ,  $^{175}\text{Lu}$ ,  $^{180}\text{Hf}$ ,  $^{181}\text{Ta}$ , and  $^{182}\text{W}$  leading to probable formation of CN in the pre-actinide region, at a laboratory energy ( $E_{\text{lab}}$ ) range of 129–146 MeV. Measurements were performed with large angular coverage ( $\theta_{\text{lab}} = 41^\circ\text{--}170^\circ$ ) in which fission fragments (FFs) were detected by nine hybrid telescope ( $E\text{-}\Delta E$ ) detectors. Extracted fission angular anisotropies and  $\sigma_{\text{fis}}$  were compared with statistical model (SM) predictions.

**Results:** Barring two reactions involving targets with large non-zero ground state spin ( $\mathcal{J}$ ), viz.,  $^{175}\text{Lu}(\frac{7}{2}^+)$  and  $^{181}\text{Ta}(\frac{7}{2}^+)$ , experimental fission angular anisotropies were found to be higher in comparison with predictions of the statistical saddle point model (SSPM), at  $E_{\text{c.m.}}$  near  $V_{\text{B}}$ . Comparison of present results with those from neighboring systems revealed that experimental anisotropies increasingly deviated from SSPM predictions as one moved from pre-actinide to actinide nuclei. For reactions involving targets with large nonzero  $\mathcal{J}$ , this deviation was subdued. Comparison between measured  $\sigma_{\text{fis}}$  and predictions of SM indicated the presence of NCNF in at least four systems, when shell effects, both in the level density and the fission barrier, were included in the calculation.

**Conclusions:** Systematic SM analysis of measured fission angular anisotropies and  $\sigma_{\text{fis}}$  confirmed the onset of NCNF in pre-actinide nuclei. Discrepancies between results about the degree of its influence on complete fusion, as deduced from various experimental probes, remain challenges to be solved. Complete measurement of all signatures of NCNF for many systems and preferably a dynamical description of the collisions between projectile and target nuclei are warranted for a deeper understanding.

DOI: [10.1103/PhysRevC.94.044607](https://doi.org/10.1103/PhysRevC.94.044607)

### I. INTRODUCTION

Production of a fully equilibrated massive compound nucleus (CN) by fusing two heavy nuclei is known to be inhibited by competing fission-like processes. Fast fission [1], quasifission [2], and pre-equilibrium fission [3], often collectively called non-CN fission (NCNF), may cause reseparation of the composite target-projectile system after its capture inside the potential barrier. The presence of NCNF in a reaction thus reduces the probability of synthesis of a heavy evaporation

residue (ER), which is the cold residual nucleus formed following evaporation of light particles and emission of  $\gamma$  rays from the excited CN. Besides suppression of ER cross sections ( $\sigma_{\text{ER}}$ ) [4–6], NCNF is reported to have other experimental signatures, viz., increase in the width of the fission fragment (FF) mass distribution [7–9] incompatible with fission of the CN (CNF), anomalous FF angular anisotropies [10,11], and FF mass-angle correlation [12]. NCNF in a reaction causes the fusion probability ( $P_{\text{CN}}$ ) to deviate from unity. Determining the NCNF cross section,  $\sigma_{\text{NCNF}}$  (or the complementary fusion cross section,  $\sigma_{\text{fis}}$ ) as a fraction of capture cross section,  $\sigma_{\text{cap}}$ , is a difficult task, especially for the less fissile systems. This is because the characteristics of the experimental observables from CNF and NCNF in these nuclei often show considerable overlap. Moreover, there are disagreements between the quanta of NCNF in a given reaction, as deduced from different experimental probes.

\*he.tatha@gmail.com

<sup>†</sup>Presently at Department of Nuclear Physics, Research School of Physical Sciences and Engineering, The Australian National University, Canberra, ACT 2601, Australia.

<sup>‡</sup>Formerly with Physics Group, Variable Energy Cyclotron Centre, 1/AF Bidhan Nagar, Kolkata 700064, India.

Banerjee *et al.* [13] recently examined ER excitation functions for 52 reactions with  $A_{\text{CN}} = 170\text{--}220$  and concluded that at least two parameters are needed to predict the onset of NCNF: one for the bulk properties of the composite system (fissility of the CN,  $\chi_{\text{CN}}$ ) and one for the entrance channel [charge product  $Z_p Z_t$  or mass asymmetry  $\eta = \frac{|A_p - A_t|}{A_p + A_t}$ ,  $Z_p$  ( $Z_t$ ) and  $A_p$  ( $A_t$ ) being the atomic number and the mass number of the projectile (target), respectively]. The authors also prescribed approximate boundaries for the onset of NCNF. These boundaries, though obtained from a robust analysis of a large data set, are somewhat model dependent and susceptible to systematic uncertainties primarily because of ambiguities in choosing SM parameters. However, it was quite evident that the transition from the domain of statistical models to that of the dynamical models occurred in pre-actinide nuclei.

In the present work, we attempt to further investigate the presence of NCNF processes in pre-actinide nuclei from FF angular distribution data. FF angular anisotropies and  $\sigma_{\text{fis}}$  in six  $^{28}\text{Si}$ -induced reactions are reported. Any deviation from the prediction of the statistical model (SM) is usually interpreted as a signature of NCNF. The experimental details are described in Sec. II. Results are presented in Sec. III followed by a discussion in Sec. IV. We summarize our findings and conclude in Sec. V.

## II. EXPERIMENTAL DETAILS

The experiment was performed at the general purpose scattering chamber (GPSC) facility of the Inter University Accelerator Centre (IUAC), New Delhi. A  $^{28}\text{Si}$  beam from the 15UD Pelletron accelerator was bombarded onto six isotopically enriched targets [14–17], details of which are presented in Table I, leading to probable formation of pre-actinide CN, viz.,  $^{197}\text{Bi}$ ,  $^{204}\text{Po}$ ,  $^{203}\text{At}$ ,  $^{208}\text{Rn}$ ,  $^{209}\text{Fr}$ , and  $^{210}\text{Ra}$ . All the targets were fabricated at the target preparation laboratory of IUAC. The target ladder was placed at the center of the cylindrical scattering chamber, tilted  $45^\circ$  with respect to the beam direction and about a vertical axis passing through the center of the target. A schematic of the experimental setup is shown in Fig. 1.

Two silicon PIPS detectors (active area  $100\text{ mm}^2$ , thickness  $300\text{ }\mu\text{m}$ , bias  $+60\text{ V}$ ) were mounted at laboratory angle ( $\theta_{\text{lab}}$ )  $10^\circ$  with respect to the beam direction in the horizontal plane and at a distance of  $70.0\text{ cm}$  from the target. Signals from these detectors were utilized for positioning the beam at the center of targets during the experiment and absolute normalization of cross sections during post-experiment analysis of data.

Nine hybrid telescope detectors [18], in two groups, were mounted on the two movable arms inside the scattering chamber: six telescopes on the upper arm covering  $\theta_{\text{lab}}$  of  $60^\circ\text{--}170^\circ$  and three telescopes on the lower arm covering  $\theta_{\text{lab}}$  of  $41^\circ\text{--}70^\circ$ . Each telescope consisted of an ionization chamber (IC) for measuring energy loss ( $\Delta E$ ) of reaction products in the front followed by a silicon detector to record the residual energy ( $E$ ) of the same at the back. The ICs, with active diameters of  $25\text{ mm}$ , were composed of three wire planes and operated with isobutane gas at a pressure of  $74\text{ mbar}$  and a bias of  $+150\text{ V}$ . The three telescopes at the forward angles had PIN diodes from Detection Technologies (active area  $100\text{ mm}^2$ ,

TABLE I. Details of the targets used in this work. All values are in the units of  $\mu\text{g}/\text{cm}^2$ .

	$^{169}_{69}\text{Tm}$	$^{176}_{70}\text{Yb}$	$^{175}_{71}\text{Lu}$	$^{180}_{72}\text{Hf}$	$^{181}_{73}\text{Ta}$	$^{182}_{74}\text{W}$
Thickness	250	150	110	150	160	70
$^{\text{nat}}\text{C}$ backing	22	25	22	40	22	22
$^{\text{nat}}\text{C}$ capping	20	20	20			

thickness  $300\text{ }\mu\text{m}$ , bias  $+30\text{ V}$ ) as the back detectors. Silicon PIPS detectors (active area  $150\text{ mm}^2$ , thickness  $300\text{ }\mu\text{m}$ , bias  $+40\text{ V}$ ) were used as the back detectors in the remaining six telescopes. Measurements were carried out keeping the telescopes at overlapping  $\theta_{\text{lab}}$ . Uncertainties in measured partial cross sections caused by uncertainties in relative solid angles of the telescopes were found to be insignificant. All the  $\Delta E$  and  $E$  detectors were coupled with custom-designed charge-sensitive preamplifiers [19] with the advantages of having low noise, high gain, low power consumption, and good timing characteristics for particle identification.

The logical OR of the timing signals from each of the detectors was the master trigger for the data acquisition system. List mode data were recorded employing IUAC's in-house data acquiring software CANDLE [20].

## III. RESULTS

### A. Fission anisotropies

Fission fragments were distinguished from other reaction products based on energy loss and residual

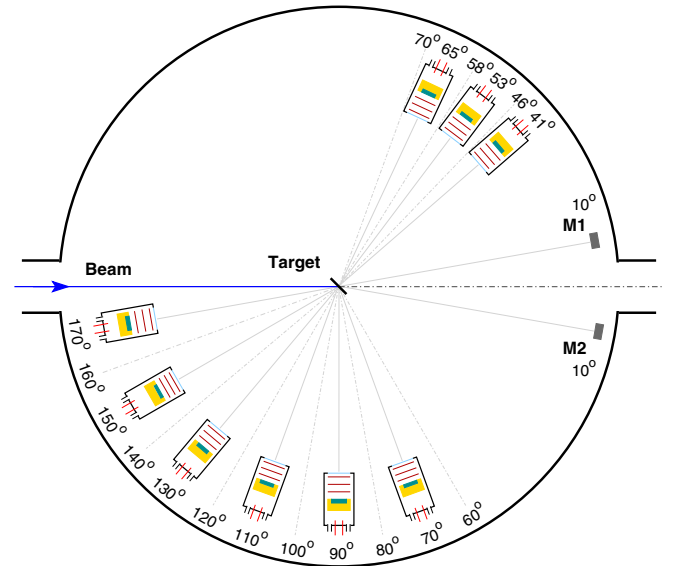


FIG. 1. Schematic of the experimental setup (top view) used for measurement of the FF angular distribution for the six  $^{28}\text{Si}$ -induced reactions. Two monitor detectors (M1 and M2) and nine hybrid telescope detectors were used in the experiment. Laboratory angles of all the detectors are mentioned in the figure. At each  $E_{\text{lab}}$  and for each reaction, FF yields were measured at seventeen angles by rotating the movable arms on which telescope detectors were mounted. The primary beam was dumped on an adequately shielded Faraday cup placed  $\sim 3\text{ m}$  downstream from the target.

energy, as shown in Fig. 2 for the reaction  $^{28}\text{Si} + ^{181}\text{Ta}$  at  $E_{\text{lab}} = 146.5$  MeV. FFs were unambiguously identified at all  $\theta_{\text{lab}}$ , except at  $170^\circ$ . Differential fission cross sections in the laboratory frame of reference,  $\frac{d\sigma_{\text{fis}}}{d\Omega}(\theta_{\text{lab}})$ , for each reaction at different  $E_{\text{lab}}$  were first determined using the Rutherford-scattering normalization. Measured angular

distributions were transformed to the center-of-mass (c.m.) frame of reference by assuming symmetric mass division and using Viola systematics [21] for FF kinetic energies. The FF angular distributions in the c.m. frame of reference,  $\frac{d\sigma_{\text{fis}}}{d\Omega}(\theta_{\text{c.m.}})$ , thus obtained, were fitted with the following exact theoretical expression [22] for the angular distribution function:

$$W(\theta) \propto \sum_{J=0}^{\infty} \sum_{M=-(I_0+s)}^{+I_0+s} \left\{ \sum_{\ell=0}^{\infty} \sum_{S=|I_0-s|}^{I_0+s} \sum_{\mu=-I_0}^{+I_0} \frac{(2\ell+1)T_\ell |C_{M,0,M}^{S,\ell,J}|^2 |C_{\mu,M-\mu,M}^{I_0,s,S}|^2}{\sum_{\ell=0}^{\infty} (2\ell+1)T_\ell} \right\} \left[ \frac{\sum_{K=-J}^J (2J+1) |d_{M,K}^J(\theta)|^2 \exp(-\frac{K^2}{2K_0^2})}{\sum_{K=-J}^J \exp(-\frac{K^2}{2K_0^2})} \right]. \quad (1)$$

Here  $I_0$  and  $s$  are target and projectile spins, respectively.  $S$  is the channel spin, defined by the relation  $\vec{S} = \vec{I}_0 + \vec{s}$ . The total angular momentum  $J$  is defined by  $\vec{J} = \vec{S} + \vec{\ell}$ , where  $\ell$  is the orbital angular momentum.  $\mu$  and  $M$  are the projections of  $\vec{I}_0$  and  $\vec{J}$  (and  $\vec{S}$ ) on the space-fixed axis whereas  $K$  is the projection of  $\vec{J}$  onto the nuclear symmetry axis. The fusion transmission coefficient for a particular orbital angular momentum  $\ell$  is given by  $T_\ell$ .  $|C_{M,0,M}^{S,\ell,J}|$  and  $|C_{\mu,M-\mu,M}^{I_0,s,S}|$  are the Clebsch-Gordan coefficients. The latter one couples the spins of target and projectile resulting in the channel spin  $\vec{S}$ , and the former one couples this  $\vec{S}$  with the orbital angular momentum  $\ell$  ending up in forming  $\vec{J}$ .  $K_0^2$  is the variance of the Gaussian  $K$  distribution and  $|d_{M,K}^J(\theta)|$  is the nontrivial rotational part of Wigner  $\mathcal{D}$  function. The measured FF angular distributions, normalized to  $W(90^\circ)$ , for the six reactions are shown in Figs. 3–8. In each case, the best fit to data was obtained by treating  $K_0^2$  as the free parameter. Effects of light particle evaporation were not included in the present calculation.

The quantity within curly brackets in Eq. (1), usually denoted by  $W(J,M)$ , is the weighting function for each possible fission channel  $(J,M)$ . In the limits  $I_0 = 0, s = 0$ , and consequently  $M = 0$ , this part disappears and Eq. (1) reduces to a simpler form. Fission angular distributions from reactions involving projectiles and/or targets with small  $\mathcal{J}$  are often fitted with the reduced form of Eq. (1) for simplicity.

The three odd-mass targets in the present work have nonzero  $\mathcal{J}$  (Table II). Butt *et al.* [23,24] reported in detail the effects of finite  $\mathcal{J}$  on fission fragment angular distributions. It was shown that measured fission anisotropies ( $A_{\text{exp}}$ ) for  $^{31}\text{P} + ^{176}\text{Lu}$  ( $\mathcal{J}^\pi = 7^+$ ) could be reproduced only when correlation of the ground state spin of  $^{176}\text{Lu}$  with the nuclear deformation axis was taken into consideration. In the present work, we did not consider deformation aligned ground state spin as  $A_{\text{cal}}$  did not change appreciably for the reaction  $^{31}\text{P} + ^{175}\text{Lu}$  ( $\frac{7}{2}^+$ ) with isotropic and aligned spin [24]. However, we investigated the differences between  $W(J)$ , calculated with the assumption  $M = 0$  and with nonzero isotropic spin. The finding is shown

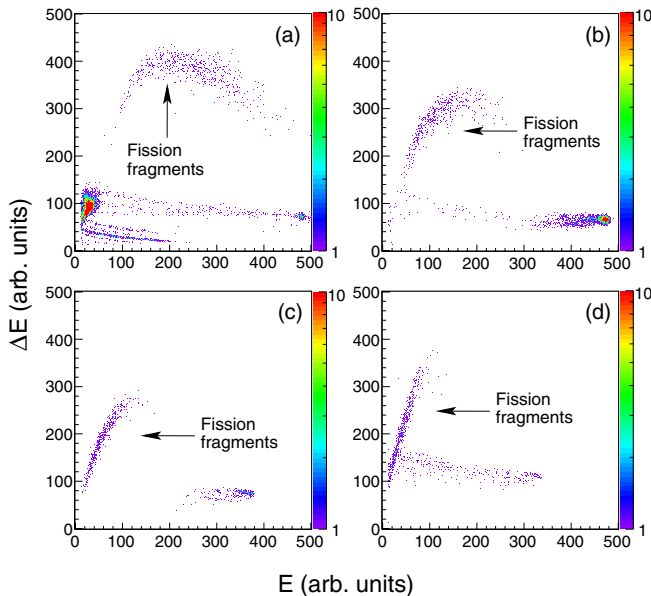


FIG. 2. Scatter plots of energy ( $E$ ) versus energy-loss ( $\Delta E$ ) of reaction products for the system  $^{28}\text{Si} + ^{181}\text{Ta}$  at  $E_{\text{lab}} = 146.5$  MeV with the hybrid telescope detectors kept at  $\theta_{\text{lab}}$  (a)  $41^\circ$ , (b)  $90^\circ$ , (c)  $130^\circ$ , and (d)  $170^\circ$ . The FFs are labeled in each panel.

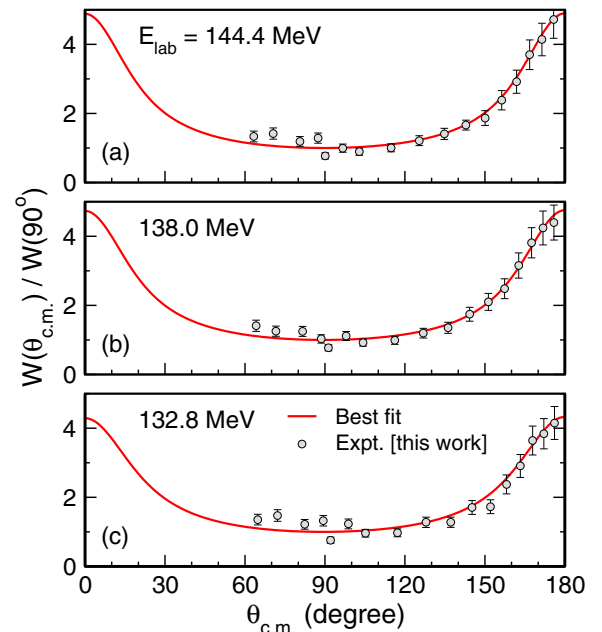


FIG. 3. Measured fission fragment angular distributions along with the best fit to data for the reaction  $^{28}\text{Si} + ^{169}\text{Tm}$ .

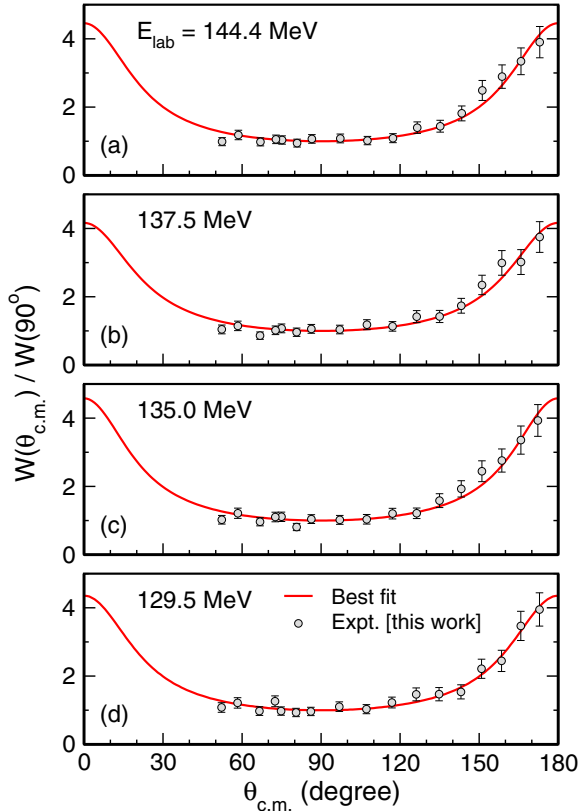


FIG. 4. Measured fission fragment angular distributions along with the best fit to data for the reaction  $^{28}\text{Si} + ^{176}\text{Yb}$ .

in Fig. 9 for the reaction  $^{28}\text{Si} + ^{175}\text{Lu}$ . Though some difference was noted between the two sets of result for  $W(J)$ , fitted angular distributions with  $M = 0$  and  $M \neq 0$  did not show any significant difference in the case of odd-mass targets.  $A_{\text{exp}}$  were obtained from the ratio  $\frac{W(180^\circ)}{W(90^\circ)}$ , in which  $W(\theta_{\text{c.m.}})$  was calculated by Eq. (1), and are presented in Table III and Fig. 10.

We may note here that  $|d_{M,K}^J(\theta)|$ , when calculated by means of the Wigner formula [22] as a polynomial of cosine and sine of half of the second Euler angle,  $\theta$ , leads to an intolerably large numerical error for large values of  $J$ . Tajima [25] recently reported a method of evaluating  $|d_{M,K}^J(\theta)|$  without loss of precision, in which the  $d$  function was expressed as the Fourier series of  $\frac{\theta}{2}$ . In our work, we adopted Tajima's prescription while evaluating  $|d_{M,K}^J(\theta)|$  in Eq. (1).

In the transition-state model of fission,  $K_0$  is given by

$$K_0^2 = \frac{\mathcal{I}_{\text{eff}}}{\hbar^2} T_{\text{sad}}, \quad (2)$$

where  $\mathcal{I}_{\text{eff}}$  is the effective moment of inertia at the saddle point. The saddle point temperature is calculated by the expression

$$T_{\text{sad}} = \left( \frac{E_{\text{c.m.}} + Q - B_f(\ell) - E_{\text{rot}}(\ell) - E_n}{a} \right)^{\frac{1}{2}}, \quad (3)$$

where  $E_{\text{c.m.}}$  is the energy in the center-of-mass (c.m.) frame of reference and  $Q$  is the  $Q$  value for formation of the CN.  $B_f(\ell)$  and  $E_{\text{rot}}(\ell)$  are the  $\ell$  dependent fission barrier and rotational

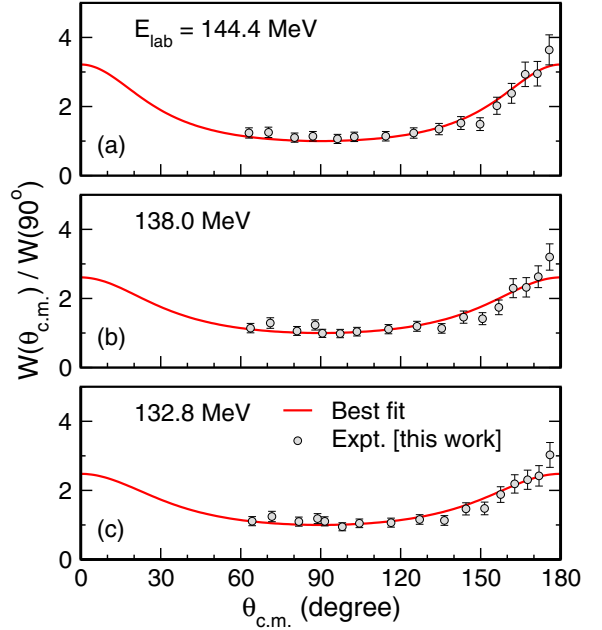


FIG. 5. Measured fission fragment angular distributions along with the best fit to data for the reaction  $^{28}\text{Si} + ^{175}\text{Lu}$ .

energy, respectively.  $E_n$  is the average energy removed by the evaporated neutrons from the CN.

In the statistical saddle point model (SSPM) [26], fission angular anisotropy is a function of  $\mathcal{I}_{\text{eff}}$ ,  $J$ , and  $T_{\text{sad}}$  and is given by the approximate expression

$$A_{\text{cal}} \approx 1 + \frac{\langle J^2 \rangle}{4K_0^2}. \quad (4)$$

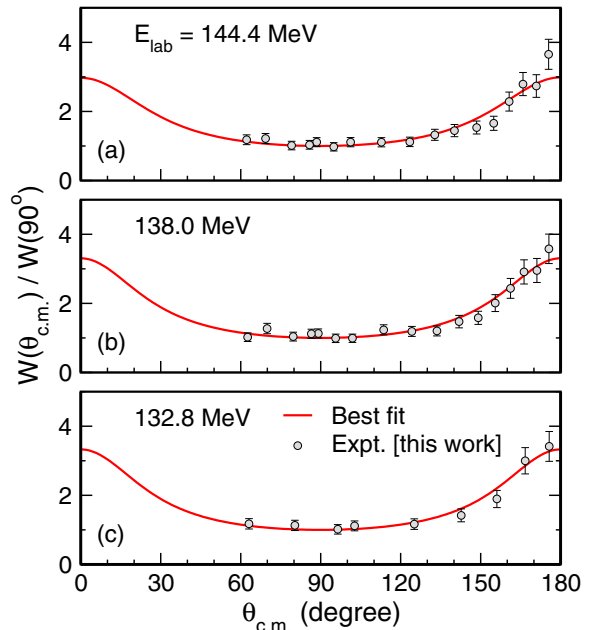


FIG. 6. Measured fission fragment angular distributions along with the best fit to data for the reaction  $^{28}\text{Si} + ^{180}\text{Hf}$ .

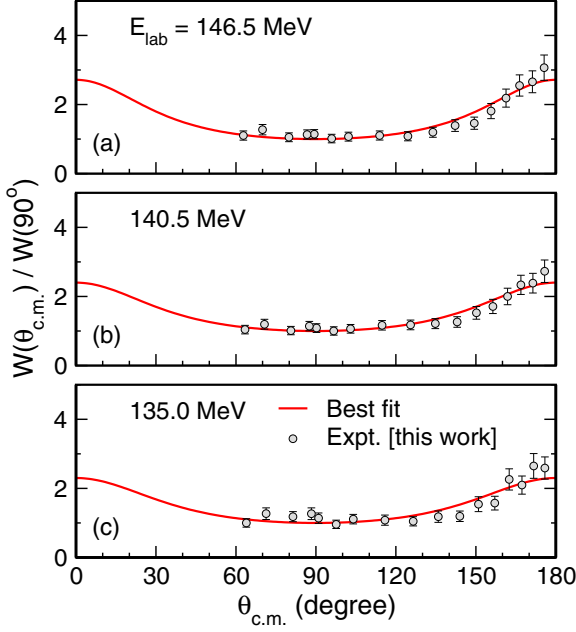


FIG. 7. Measured fission fragment angular distributions along with the best fit to data for the reaction  $^{28}\text{Si} + ^{181}\text{Ta}$ .

$\mathcal{I}_{\text{eff}}$ ,  $B_f(\ell)$ , and  $E_{\text{rot}}(\ell)$  were calculated by the rotating finite range model (RFRM) of Sierk [27] while evaluating  $A_{\text{cal}}$ .  $E_n$  was calculated using the systematics of Itkis [28]. The mean of the square of total angular momentum,  $\langle J^2 \rangle$ , of the fissioning nucleus was calculated in two steps. First, the capture  $\ell$  distribution for the reaction was obtained from the coupled-channels code CCFULL [29]. Next,  $\langle J^2 \rangle$  was calculated using the statistical model code PACE3 [30] in trace-back mode

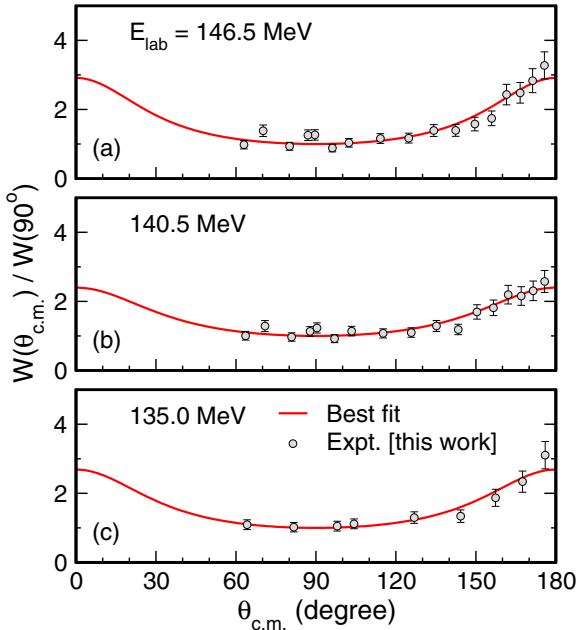


FIG. 8. Measured fission fragment angular distributions along with the best fit to data for the reaction  $^{28}\text{Si} + ^{182}\text{W}$ .

TABLE II. Deformation parameters [31–33] used in coupled-channels calculation with CCFULL.  $\mathcal{J}^\pi$  is the ground state spin and parity of the projectile and the target nuclei.

	$^{28}\text{Si}$	$^{169}\text{Tm}$	$^{176}\text{Yb}$	$^{175}\text{Lu}$	$^{180}\text{Hf}$	$^{181}\text{Ta}$	$^{182}\text{W}$
$\beta_2$	-0.407	0.294	0.306	0.287	0.274	0.269	0.259
$\beta_4$	0.25	-0.016	-0.071	-0.069	-0.096	-0.090	-0.084
$\mathcal{J}^\pi$	$0^+$	$\frac{1}{2}^+$	$0^+$	$\frac{7}{2}^+$	$0^+$	$\frac{7}{2}^+$	$0^+$

using the  $\ell$  distribution from CCFULL as the input. The level density parameter ( $a$ ), ratio of  $a$  at the saddle point to that in the ground state ( $\frac{a_f}{a_n}$ ), and the scaling factor for the RFRM fission barrier ( $k_f$ ) were taken as  $\frac{A}{10}$ , 1.00, and 1.00, respectively, in the PACE3 calculation.

It was important to verify reliability of the capture  $\ell$  distribution used in our calculation. This is usually achieved by reproducing the experimental capture excitation functions. We must mention here that the capture cross section for any reaction at a given  $E_{\text{c.m.}}$  can be divided into three components:

$$\sigma_{\text{cap}} = \sigma_{\text{ER}} + \sigma_{\text{CNF}} + \sigma_{\text{NCNF}}, \quad (5)$$

where the three terms on the right-hand side of Eq. (5) stand for ER, CNF, and NCNF cross sections, respectively. We also note that CNF and NCNF events were indistinguishable in the present experimental setup. It then follows from these facts that measured  $\sigma_{\text{fis}}$  can be considered as  $\sigma_{\text{cap}}$  if  $\sigma_{\text{ER}}$  is insignificant. We indeed estimated (upper limits of)  $\sigma_{\text{ER}}$ , within the framework of SM (discussed in Sec. III B), and found those to be comparable with the uncertainties in measured  $\sigma_{\text{fis}}$  for four reactions, viz.,  $^{28}\text{Si} + ^{175}\text{Lu}$ ,  $^{28}\text{Si} + ^{180}\text{Hf}$ ,  $^{28}\text{Si} + ^{181}\text{Ta}$ , and  $^{28}\text{Si} + ^{182}\text{W}$ . Therefore, we reproduced measured fission excitation functions for these reactions (Fig. 11) using CCFULL to produce the capture  $\ell$  distribution. For the remaining two reactions, viz.,  $^{28}\text{Si} + ^{169}\text{Tm}$  and  $^{28}\text{Si} + ^{176}\text{Yb}$ , we relied upon CCFULL predictions. Potential parameters, i.e., depth  $V_0$ , radius  $r_0$ , and diffuseness  $a$ , were obtained from the Woods-Saxon parametrization of the Akyüz-Winther potential for all the reactions except  $^{28}\text{Si} + ^{175}\text{Lu}$  and  $^{28}\text{Si} + ^{181}\text{Ta}$ , for which a deeper potential well ( $V_0 = 82$  MeV) was required to reproduce measured excitation functions. The projectile  $^{28}\text{Si}$  was treated as oblate deformed [35,36]. The deformation parameters used in coupled-channels calculation are listed in Table II. For each odd-mass target, deformation parameters and energy of the first  $2^+$  excited state were approximated by averaging the corresponding values in neighboring even-even nuclei.

$A_{\text{cal}}$ , thus calculated, are also plotted in Fig. 10. Uncertainties in  $A_{\text{cal}}$ , that may arise as a consequence of reasonable variations in the input parameters of PACE3, are addressed in Sec. IV.

## B. Fission cross sections

The experimental  $\sigma_{\text{fis}}$  for the six reactions were obtained by integrating the measured  $\frac{d\sigma_{\text{fis}}}{d\Omega}(\theta_{\text{c.m.}})$ . Measured fission excitation functions are shown in Fig. 12 and the cross sections are listed in Table III. The PACE3 predictions (with  $a = \frac{A}{10}$ ,

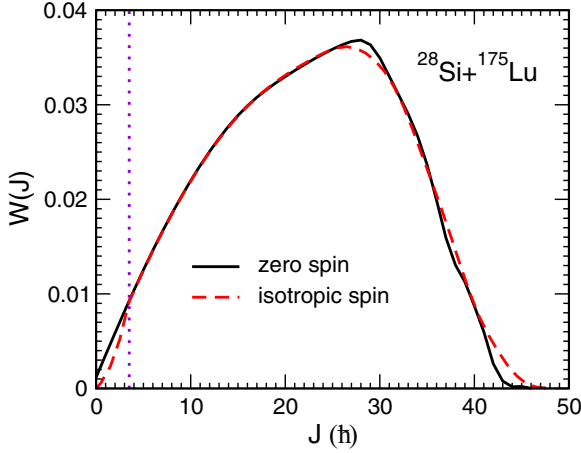


FIG. 9. The  $J$  distribution,  $W(J)$ , for the reaction  $^{28}\text{Si} + ^{175}\text{Lu}$ , calculated at  $E_{\text{lab}} = 132.8$  MeV. One may notice depletion of the distribution at  $J < \frac{7}{2}\hbar$  (left of the dotted line) when  $\mathcal{J}$  is nonzero, compared to the case with  $\mathcal{J} = 0$ .

$\frac{a_t}{a_p} = 1.00$ , and  $k_f = 1.00$ ) are also shown in this figure. No shell effects were considered in the PACE3 calculations. The PACE3 results are found to be very close to the experimental excitation functions of all the systems except  $^{28}\text{Si} + ^{180}\text{Hf}$ , where the calculated values are larger than the experimental cross sections.

We next performed SM calculations using the code VECSTAT [37], in which shell effects in the fission barrier and the nuclear level density parameter were included. In this code, evaporation of light particles (proton, neutron, and  $\alpha$

TABLE III. Measured fission cross sections and fission angular anisotropies. Energy in the center-of-mass frame of reference ( $E_{\text{c.m.}}$ ) and the excitation energy ( $E^*$ ) were calculated at the center of the target.

CN	$E_{\text{c.m.}}$ (MeV)	$E^*$ (MeV)	$\sigma_{\text{fis}}$ (mb)	$A_{\text{exp}}$
$^{197}_{83}\text{Bi}_{114}$	113.4	50.3	$64.8 \pm 7.8$	$4.33 \pm 0.52$
	117.9	54.8	$146.3 \pm 17.6$	$4.76 \pm 0.57$
	123.4	60.3	$235.6 \pm 42.4$	$4.90 \pm 0.59$
$^{204}_{84}\text{Po}_{120}$	111.5	54.8	$29.2 \pm 4.7$	$4.29 \pm 0.51$
	116.2	59.6	$108.5 \pm 13.0$	$4.58 \pm 0.55$
	118.4	61.7	$146.4 \pm 17.6$	$4.12 \pm 0.49$
	124.3	67.7	$330.1 \pm 52.8$	$4.42 \pm 0.53$
$^{203}_{85}\text{At}_{118}$	114.3	49.8	$72.0 \pm 8.6$	$2.48 \pm 0.30$
	118.8	54.3	$186.6 \pm 22.4$	$2.61 \pm 0.31$
	124.3	59.8	$319.6 \pm 38.4$	$3.22 \pm 0.39$
$^{208}_{86}\text{Rn}_{122}$	116.6	54.9	$64.8 \pm 7.8$	$3.30 \pm 0.40$
	121.3	59.7	$167.6 \pm 20.1$	$3.28 \pm 0.40$
	126.5	64.9	$333.9 \pm 40.1$	$2.98 \pm 0.36$
	121.4	55.2	$166.8 \pm 20.0$	$2.40 \pm 0.29$
$^{209}_{87}\text{Fr}_{122}$	116.6	50.4	$71.4 \pm 8.6$	$2.30 \pm 0.28$
	121.4	55.2	$166.8 \pm 20.0$	$2.40 \pm 0.29$
	126.6	60.4	$328.4 \pm 39.4$	$2.72 \pm 0.33$
	116.9	49.9	$52.0 \pm 6.2$	$2.66 \pm 0.32$
$^{210}_{88}\text{Ra}_{122}$	116.9	49.9	$52.0 \pm 6.2$	$2.66 \pm 0.32$
	121.6	54.6	$138.0 \pm 16.6$	$2.39 \pm 0.29$
	126.8	59.8	$305.9 \pm 49.0$	$2.90 \pm 0.35$

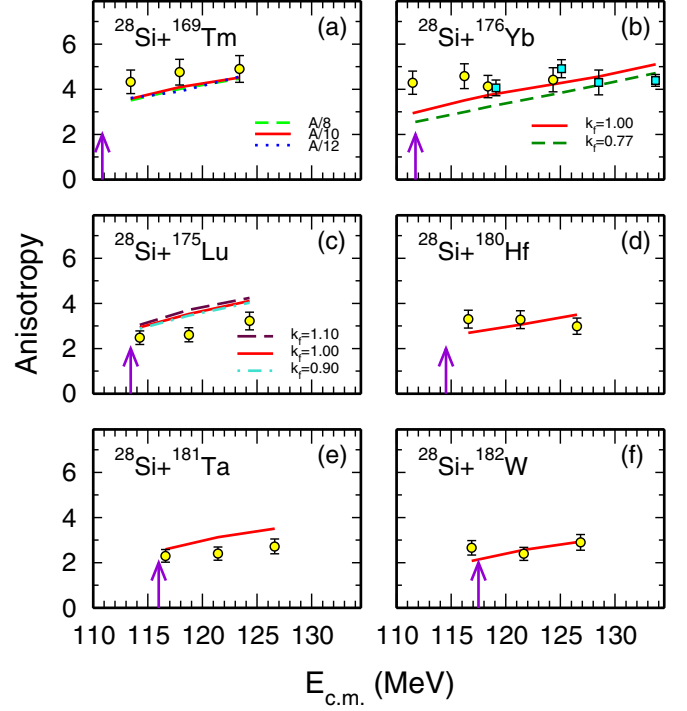


FIG. 10. Measured and calculated fission angular anisotropies for six  $^{28}\text{Si}$ -induced reactions. The default parameters in the PACE3 calculation were  $a = \frac{A}{10}$ ,  $\frac{a_t}{a_n} = 1.00$ , and  $k_f = 1.00$ . Variation in  $A_{\text{cal}}$  with  $a$  is shown in panel (a). The data points shown with solid squares in panel (b) are taken from Ref. [34]. Variation in  $A_{\text{cal}}$  caused by varying RFRM fission barrier is shown in panels (b) and (c). See text for further details.

particle) and statistical  $\gamma$  rays were considered as possible decay channels of a CN in addition to fission. While the particle and  $\gamma$  emission widths were obtained using the standard prescriptions as given in Ref. [38], the fission width was calculated from the transition-state theory of nuclear fission due to Bohr and Wheeler [39]. The Bohr-Wheeler fission width for a nucleus with total excitation energy  $\mathcal{E}$ , measured with respect to the ground state mass of the CN, and angular momentum  $\ell$  is given as

$$\Gamma_{\text{BW}}(\mathcal{E}, \ell) = \frac{1}{2\pi \rho_g(E^*)} \int_0^{E^* - B_f(\ell)} \rho_s(E^* - B_f(\ell) - \epsilon) d\epsilon, \quad (6)$$

where  $E^*$  is the intrinsic or thermal part of  $\mathcal{E}$  and is given as  $E^* = \mathcal{E} - E_{\text{rot}}(\ell) - E_{\text{pair}}$ ,  $E_{\text{rot}}(\ell)$  and  $E_{\text{pair}}$  being the rotational and the pairing energies, respectively. The level densities at the ground state and the saddle configuration are denoted by  $\rho_g$  and  $\rho_s$ , respectively.  $B_f(\ell)$  is the angular momentum dependent fission barrier. The fission width used in VECSTAT was finally obtained as

$$\Gamma_f(\mathcal{E}, \ell) = \frac{\hbar \omega_g(\ell)}{\mathcal{T}} \Gamma_{\text{BW}}(\mathcal{E}, \ell) \quad (7)$$

where  $\Gamma_{\text{BW}}(\mathcal{E}, \ell)$  was multiplied by the phase-space factor  $\frac{\hbar \omega_g(\ell)}{\mathcal{T}}$  to account for the collective degrees of freedom in the

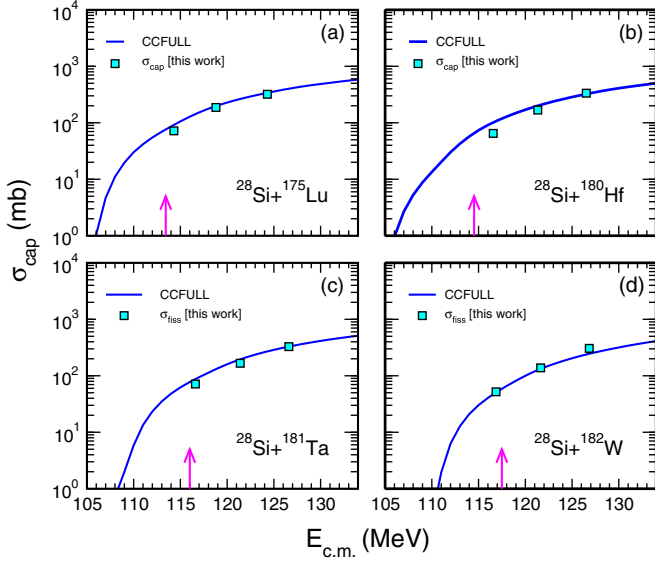


FIG. 11. Experimental and theoretical  $\sigma_{\text{cap}}$  for (a)  $^{28}\text{Si} + ^{175}\text{Lu}$ , (b)  $^{28}\text{Si} + ^{180}\text{Hf}$ , (c)  $^{28}\text{Si} + ^{181}\text{Ta}$ , and (d)  $^{28}\text{Si} + ^{182}\text{W}$  reactions. The vertical arrow in each panel indicates the position of the Coulomb barrier.

ground state [40]. Here  $\omega_g(\ell)$  is the frequency of a harmonic oscillator potential having the same curvature of the nuclear potential at the ground state and  $\mathcal{T}$  is the nuclear temperature.

The fission barrier  $B_f(\ell)$  in the present calculation was obtained by incorporating a shell correction in the liquid-drop nuclear mass [41]. The shell correction term  $\delta W$  is given as the difference between the experimental and the liquid-drop model (LDM) masses ( $\delta W = M_{\text{exp}} - M_{\text{LDM}}$ ). The fission barrier then is given as

$$B_f(E^*, \ell) = B_f^{\text{LDM}}(E^*, \ell) - (\delta W_g - \delta W_s) \quad (8)$$

where  $B_f^{\text{LDM}}(E^*, \ell)$  is the angular momentum dependent LDM fission barrier and  $\delta W_g$  and  $\delta W_s$  are the shell correction energies for ground state and saddle configurations, respectively.  $B_f^{\text{LDM}}(E^*, \ell)$  was obtained from the finite range liquid drop model (FRLDM) potential [27] and  $\delta W_g$  was taken from Ref. [42]. For small  $\ell$ , the fission barrier is high and the nuclear shape at the saddle is highly deformed. In such cases, we neglected the shell correction at the saddle deformation ( $\delta W_s$ ) following the topological argument forwarded by Myers and Swiatecki [43]. However, with increasing  $\ell$ , the saddle configuration becomes more compact and, for a large value of  $\ell$  where the LDM fission barrier vanishes, the ground state and the saddle configurations become infinitesimally close to each other. Consequently, the shell correction term should vanish in the above limiting condition. It thus appears that there should be a scaling of the shell correction term as the saddle point moves closer to the ground state configuration with increasing  $\ell$ . We therefore introduced a scaling factor  $f_\ell$  in the shell correction term and obtained the fission barrier as

$$B_f(E^*, \ell) = B_f^{\text{LDM}}(E^*, \ell) - f_\ell \delta W_g, \quad (9)$$

where  $f_\ell = 1$  for  $\ell = 0$  and  $f_\ell \rightarrow 0$  for large  $\ell$ . We used the ansatz  $f_\ell = \frac{B_f^{\text{LDM}}(\ell)}{B_f^{\text{LDM}}(\ell=0)}$  in the present calculation.

The intensity of various decay modes of a CN depends critically on the density of levels of the parent and the daughter nuclei. The level density in turn is a sensitive function of the level density parameter ( $a$ ), which was taken from the work of Ignatyuk *et al.* [44]. In this prescription,  $a$  includes shell effects at low excitation energies and goes over to its asymptotic form at high excitation energies,

$$a(E^*) = \tilde{a} \left( 1 + \frac{f(E^*)}{E^*} \delta W \right), \quad (10)$$

with  $f(E^*) = 1 - \exp(-\frac{E^*}{E_D})$  where  $\tilde{a}$  is the asymptotic level density and  $E_D$  is a parameter which decides the rate at which the shell effects disappear with an increase in  $E^*$ . A value of 18.5 MeV was used for  $E_D$ , which was obtained from an analysis of  $s$ -wave neutron resonances [45]. The shape dependent asymptotic level density was also taken from Ref. [45]

The capture  $\ell$  distributions obtained from CCFULL treating  $^{28}\text{Si}$  as oblate deformed were used as input CN  $\ell$  distributions in VECSTAT. The calculated fission excitation functions from VECSTAT are also shown in Fig. 12. The calculated values are lower than the experimental values for most of the systems. In particular, the VECSTAT-predicted  $\sigma_{\text{fis}}$  for  $^{28}\text{Si} + ^{176}\text{Yb}$  are substantially smaller than the experimental values.  $\sigma_{\text{fis}}$  were also obtained from VECSTAT without considering shell effects in the fission barrier as well as the level density parameter. These calculated cross sections were very close to the PACE3 predictions, as expected (Fig. 12). Inclusion of shell effects thus lowered the fission cross sections.

#### IV. DISCUSSION

We first examine in detail the uncertainties in  $A_{\text{cal}}$  because of the variation in input parameters of PACE3. The parameters  $a$ ,  $\frac{a_f}{a_n}$ , and  $k_f$  are often adjusted to reproduce experimental observables. Ramachandran *et al.* [46] had measured pre-scission neutron, proton, and  $\alpha$ -particle multiplicities for  $^{28}\text{Si} + ^{175}\text{Lu}$ . In order to explain observed multiplicities, a fission barrier of 1.10 times the RFRM barrier [27] was used in the SM calculation. Hinde *et al.* [47] considered  $a = \frac{A}{10}$  and  $\frac{a_f}{a_n} = 1.00$  for successful reproduction of  $\sigma_{\text{ER}}$  or neutron multiplicity. On the other hand, to avoid overprediction in charged particle multiplicity, Lestone *et al.* [48] had to take  $a < \frac{A}{10}$  and  $\frac{a_f}{a_n} > 1.00$ . Mahata *et al.* [49] showed that ER and fission excitation functions were less sensitive to  $B_f$  and  $\frac{a_f}{a_n}$ , whereas pre-saddle neutron multiplicity and fission angular anisotropy were more sensitive to these parameters. Different combinations of  $B_f$  and  $\frac{a_f}{a_n}$  could give equally good fits to the excitation functions. Saxena *et al.* [50] found the use of  $a = \frac{A}{10}$  fruitful in describing experimental neutron and  $\alpha$ -particle spectra and pre-scission and post-scission multiplicities. The same value of  $a$  was used by Ikezoe *et al.* [51] for reproducing pre- and post-scission multiplicities of protons and  $\alpha$  particles. In a comprehensive SM analysis of ER and fission excitation functions and spectral shapes of evaporated  $\alpha$  particles in

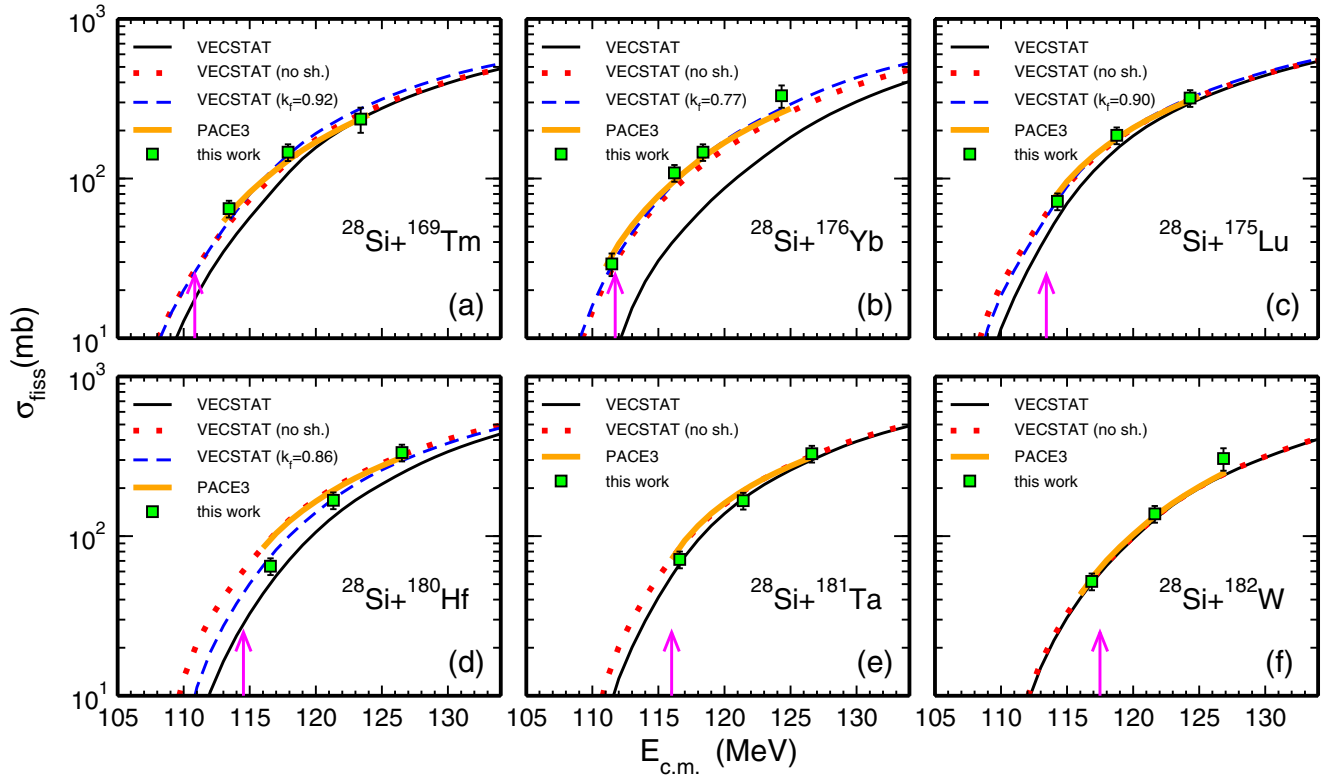


FIG. 12. Measured and calculated  $\sigma_{\text{fis}}$  for (a)  $^{28}\text{Si}+^{169}\text{Tm}$ , (b)  $^{28}\text{Si}+^{176}\text{Yb}$ , (c)  $^{28}\text{Si}+^{175}\text{Lu}$ , (d)  $^{28}\text{Si}+^{180}\text{Hf}$ , (e)  $^{28}\text{Si}+^{181}\text{Ta}$ , and (f)  $^{28}\text{Si}+^{182}\text{W}$ . Data points from the present work are shown with solid squares. The (black) continuous lines represent VECSTAT predictions whereas the thick (orange) continuous lines show the result from PACE3. The (blue) dashed lines are the predictions of VECSTAT with a scaled-down LDM fission barrier. The (red) dotted lines show results from VECSTAT when shell effects were not included in the calculation. The vertical arrow in each panel indicates position of the Coulomb barrier. See text for further details.

$^{19}\text{F}+^{181}\text{Ta}$ , Caraley *et al.* [52] used  $k_f = 1.00$ ,  $\frac{a_f}{a_n} = 1.04$ , and moderate temperature dependence in the level density parameter in the range from  $a = \frac{A}{10.5}$  to  $a = \frac{A}{12}$ . In the present work,  $a = \frac{A}{10}$ ,  $\frac{a_f}{a_n} = 1.00$ , and  $k_f = 1.00$  were used in the PACE3 calculation. Nevertheless, the variations in  $A_{\text{cal}}$ , due to reasonable changes in these parameters were also investigated. Figure 10(a) shows changes in  $A_{\text{cal}}$  with different values of  $a$ . Likewise, the effect of variation in fission barrier (in other words,  $k_f$ ) on  $A_{\text{cal}}$  is shown in Figs. 10(b) and 10(c). No significant changes in  $A_{\text{cal}}$  were noticed except for the case with  $k_f = 0.77$ .

In the case of reactions involving  $^{169}\text{Tm}$ ,  $^{176}\text{Yb}$ ,  $^{180}\text{Hf}$  and  $^{182}\text{W}$ , targets,  $A_{\text{cal}}$  deviates from  $A_{\text{exp}}$  when going towards  $V_B$ . The obvious reason for this is structural effects, as was explained by Hinde *et al.* [53]. Fusion-fission and quasifission start competing with each other from this mass region. A range of fusion barrier radii are involved in the reactions. At  $E_{\text{c.m.}}$  near and below  $V_B$ , the entrance channel  $K$  distribution is narrow and peaks close to  $K' = J \sin \omega$  ( $\omega$  being the angle of orientation of the target nucleus with respect to beam direction during capture) preferring tip-to-tip collision of deformed nuclei and in effect increasing  $I_{\text{eff}}$ . This strong influence makes  $A_{\text{exp}}$  higher than SSPM predictions. But, at  $E_{\text{lab}}$  above  $V_B$ , the entrance channel  $K$  distribution for each  $J$  is uniform and broad enough not to be influenced by the  $K$ -state equilibration severely. In other words, the dinuclear system gets more

compact, resulting in a larger fraction of CNF. Thus  $A_{\text{exp}}$  comes closer to SSPM predictions at  $E_{\text{c.m.}}$  above  $V_B$ .

The effect of nonzero  $\mathcal{J}$  (of target and/or projectile) on FF angular distribution and anisotropy is a long known fact [23,24,54–57]. In the case of nonzero  $\mathcal{J}$ , the entrance channel  $K$  distribution does not peak at  $K' = J \sin \omega$ , but at  $K' = J \sin \omega \pm \mathcal{J}$  which results in a lowering of anisotropies [56].  $A_{\text{cal}}$  for the two reactions involving  $^{175}\text{Lu}$  and  $^{181}\text{Ta}$  exceeded  $A_{\text{exp}}$ , as shown in Figs. 10(c) and 10(e).

We plotted  $\frac{A_{\text{exp}}-1}{A_{\text{cal}}-1}$  for the current systems as well as six more  $^{28}\text{Si}$ -induced reactions in Fig. 13. The ratio exceeds unity as one moves towards the Coulomb barrier (increasing the probability of tip-to-tip collisions) and from lighter to heavier targets (increasing CN fissility and entrance channel mass asymmetry), indicating departure from SSPM predictions. This deviation also signifies the presence of NCNF in a system. However, one may also observe exceptions to this general trend upon closer scrutiny of Fig. 13. Departure of the ratio  $\frac{A_{\text{exp}}-1}{A_{\text{cal}}-1}$  from unity is subdued for systems involving targets with large  $\mathcal{J}$ , e.g.,  $^{175}\text{Lu}(\frac{7}{2}^+)$  and  $^{181}\text{Ta}(\frac{7}{2}^+)$ , as already mentioned. This point is further highlighted in Fig. 14, in which  $\frac{A_{\text{exp}}-1}{A_{\text{cal}}-1}$  is plotted for reactions involving different projectiles on  $^{175}\text{Lu}$ ,  $^{181}\text{Ta}$ , and  $^{182}\text{W}$  targets. The ratio does not exceed unity in the case of reactions involving the first two targets [panels (a) and (b)] even when one moves from lighter to heavier projectiles.

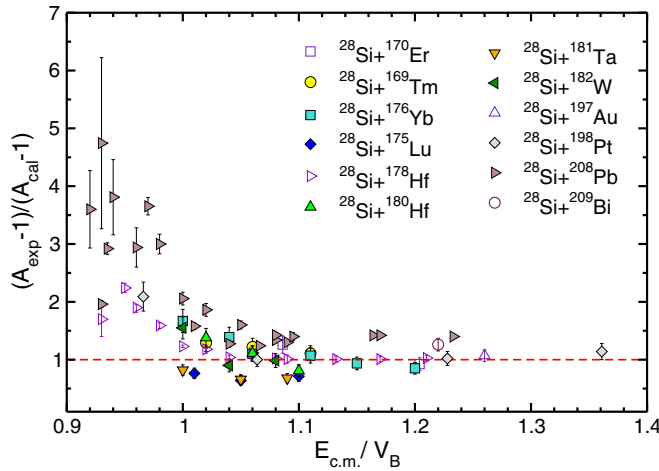


FIG. 13.  $\frac{A_{\text{exp}}^{-1}}{A_{\text{cal}}^{-1}}$  as a function of  $\frac{E_{\text{c.m.}}}{V_B}$  for reactions involving  $^{28}\text{Si}$  projectiles on various targets. Data for systems other than the present ones were obtained from literature:  $^{28}\text{Si} + ^{170}\text{Er}$  [58],  $^{28}\text{Si} + ^{176}\text{Yb}$  [34],  $^{28}\text{Si} + ^{178}\text{Hf}$  [24],  $^{28}\text{Si} + ^{197}\text{Au}$  [59],  $^{28}\text{Si} + ^{198}\text{Pt}$  [60],  $^{28}\text{Si} + ^{208}\text{Pb}$  [10,35,61],  $^{28}\text{Si} + ^{209}\text{Bi}$  [59]. For all the reactions,  $A_{\text{cal}}$  has been calculated treating  $^{28}\text{Si}$  as oblate deformed in CCFULL and considering  $a = \frac{A}{10}$ ,  $\frac{a_f}{a_n} = 1.00$ , and  $k_f = 1.00$  in PACE3.

However, for reactions involving the third target  $^{182}\text{W}$  ( $0^+$ ),  $\frac{A_{\text{exp}}^{-1}}{A_{\text{cal}}^{-1}}$  exceeds unity as one approaches  $V_B$ . Also, departure of the ratio from unity increases with increasing mass of the projectile.

Regarding SM analysis of fission excitation functions, we first note in Fig. 12 that both PACE3 and VECSTAT give reasonable fits to experimental data for all the systems except  $^{28}\text{Si} + ^{180}\text{Hf}$  when no shell effects were considered in the calculations. However, shell effects contribute to the ground state energy of a nucleus as well as to the nuclear level density at low excitation energies. The importance of shell effects in nuclear fission had also been demonstrated [70]. We therefore included shell effects in defining both the fission barrier and nuclear level density in VECSTAT, and the calculated results

were found to underestimate measured  $\sigma_{\text{fis}}$  in most cases (Fig. 12).

In the past, measured values of  $\sigma_{\text{fis}}$  had been found to exceed SM predictions (or conversely, measured  $\sigma_{\text{ER}}$  had fallen short of the theoretical values) and such observations were often interpreted as manifestations of reduction in the LDM fission barrier [71–74]. For example, Sagaidak and Andreyev [73] had reported calculated fission excitation function for  $^{16}\text{O} + ^{188}\text{Os}$  leading to the CN  $^{204}\text{Po}$ . Measured  $\sigma_{\text{fis}}$  were reproduced by scaling down the LDM fission barrier by a factor ( $k_f$ ) of 0.77. We observed that a similar scaling factor was required for SM predictions with shell effects to fit the measured fission excitation function for  $^{28}\text{Si} + ^{176}\text{Yb}$  leading to formation of the same CN ( $^{204}\text{Po}$ ). For the other reactions studied in this work, a reduction of the LDM fission barrier was required to reproduce measured  $\sigma_{\text{fis}}$  except for the systems  $^{28}\text{Si} + ^{181}\text{Ta}$  and  $^{28}\text{Si} + ^{182}\text{W}$ . The CN formed in these two reactions, viz.,  $^{209}\text{Fr}$  and  $^{210}\text{Ra}$ , are highly fissile and the calculated  $\sigma_{\text{fis}}$  consumes almost the entire input  $\sigma_{\text{cap}}$ . Also, the calculated fission excitation functions, both with and without shell effects, are indistinguishable for  $^{28}\text{Si} + ^{182}\text{W}$ .

It may, however, be remarked that reduction in the LDM fission barrier to reproduce a single experimental observable in a limited number of reactions may lead to erroneous conclusions. One may notice in Fig. 10(b) that  $A_{\text{cal}}$  in  $^{28}\text{Si} + ^{176}\text{Yb}$  is reduced significantly and thereby worsening the fit to  $A_{\text{exp}}$ , if the RFRM fission barrier is scaled down by the factor 0.77. Moreover, the probable role of NCNF in enhancing measured  $\sigma_{\text{fis}}$  (or suppressing measured  $\sigma_{\text{ER}}$ ) in comparison with SM prediction is completely ignored in the above approach. The enhancement (suppression) of  $\sigma_{\text{fis}}$  ( $\sigma_{\text{ER}}$ ) may also be interpreted as caused by the presence of NCNF, which in turn causes  $P_{\text{CN}}$  to deviate from unity. Results from other experimental probes indicate that the latter approach has sufficient justification. For example, the recent observation of enhanced mass distribution width ( $\sigma_m$ ) by Shamlath *et al.* [9] in  $^{30}\text{Si} + ^{180}\text{Hf}$  in comparison with SSPM prediction points to the presence of NCNF in this reaction. The fact that  $\sigma_m$  from the reaction  $^{16}\text{O} + ^{194}\text{Pt}$  leading to the same CN could be reproduced by SSPM calculation reveals the role of

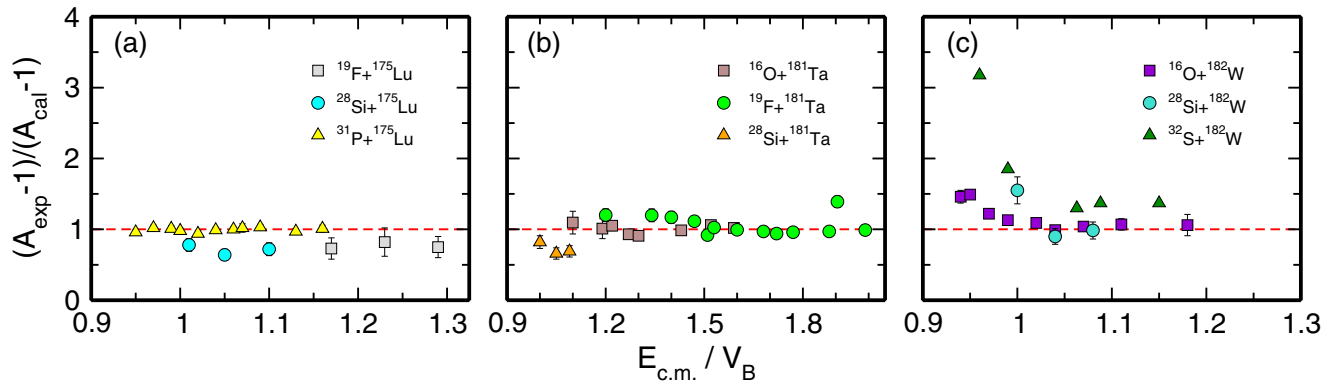


FIG. 14.  $\frac{A_{\text{exp}}^{-1}}{A_{\text{cal}}^{-1}}$  as a function of  $\frac{E_{\text{c.m.}}}{V_B}$  for reactions involving different projectiles and (a)  $^{175}\text{Lu}$ , (b)  $^{181}\text{Ta}$ , and (c)  $^{182}\text{W}$  targets. Data for systems other than the present ones were obtained from literature:  $^{19}\text{F} + ^{175}\text{Lu}$  [62],  $^{31}\text{P} + ^{175}\text{Lu}$  [24],  $^{16}\text{O} + ^{181}\text{Ta}$  [63–65],  $^{19}\text{F} + ^{181}\text{Ta}$  [51,66],  $^{16}\text{O} + ^{182}\text{W}$  [67],  $^{32}\text{S} + ^{182}\text{W}$  [68,69]. For all reactions barring  $^{28}\text{Si}$ -induced ones and  $^{19}\text{F} + ^{175}\text{Lu}$ ,  $A_{\text{exp}}$  and  $A_{\text{cal}}$  were taken from the same reference in each case.

entrance channel dynamics in the observed deviation in case of  $^{30}\text{Si} + ^{180}\text{Hf}$ . Therefore, the SM description of the outcome of a fusion reaction in this mass region, requiring drastic variation of the LDM fission barrier to reproduce a set of cross sections, may not be adequate. Rather, a dynamical model description of the reaction process would be more appropriate. Similar conclusions were drawn in a few other recent works [13,75].

Finally, we look for signatures of NCNF, if any, in the current reactions. Deviation of  $A_{\text{exp}}$  from SSPM predictions near  $V_B$  indicates presence of NCNF in the system. For reactions involving odd-mass targets with large  $\mathcal{J}$  ( $^{175}\text{Lu}$  and  $^{181}\text{Ta}$ ), we found this signature to be clearly subdued. Therefore, concluding about the presence of NCNF in a particular reaction, based on fission angular anisotropy alone, may be incorrect. The fact that the measured  $\sigma_{\text{fis}}$  are larger than VECSTAT predictions for four reactions can be interpreted as a signature of NCNF. Statistical models, inherently, assume  $P_{\text{CN}}$  to be unity. Therefore, measured  $\sigma_{\text{fis}}$  in excess of calculated  $\sigma_{\text{fis}}$  must have non-CN origin. Four reactions, for which measured fission excitation functions exceed VECSTAT predictions [Figs. 12(a)–12(d)], thus reveal the presence of NCNF. Since, measured fission excitation functions for the two remaining systems, viz.,  $^{28}\text{Si} + ^{181}\text{Ta}$  and  $^{28}\text{Si} + ^{182}\text{W}$ , could be reproduced satisfactorily by VECSTAT, the presence of NCNF in these two reactions appears to be insignificant. We note that these two are the most asymmetric reactions among the six systems studied in this work. Also,  $^{181}\text{Ta}$  and  $^{182}\text{W}$  are the least deformed among the six targets, having the lowest quadrupole deformation parameters (listed in Table II). These could be among the probable reasons for nonobservation of clear signatures of NCNF in  $^{28}\text{Si} + ^{181}\text{Ta}$  and  $^{28}\text{Si} + ^{182}\text{W}$ . Study with other experimental probes and calculation by a suitable dynamical model may reveal the extent of NCNF in such cases.

## V. CONCLUSIONS

We measured the FF angular distribution for six reactions induced by  $^{28}\text{Si}$  projectiles at and above  $V_B$ , leading to probable formation of pre-actinide CN. Fission angular anisotropy and  $\sigma_{\text{fis}}$  were extracted from the data. Uncertainties in  $A_{\text{cal}}$

that may be caused by reasonable variation of the input parameters of SM were thoroughly investigated and were found to be insignificant.  $A_{\text{exp}}$  were found to be higher than SSPM predictions at  $E_{\text{c.m.}}$  near  $V_B$ , except for the two reactions involving odd-mass targets with large nonzero  $\mathcal{J}$ , viz.,  $^{175}\text{Lu} (\frac{7}{2}^+)$  and  $^{181}\text{Ta} (\frac{7}{2}^+)$ . We compared the current results with fission angular anisotropies from neighbouring systems. The comparison revealed that  $A_{\text{exp}}$ , in general, increasingly exceeded SSPM predictions with increasing entrance channel mass asymmetry and mass of the composite system. Deviations of  $A_{\text{exp}}$  from SSPM predictions were found to be subdued, in the case of reactions involving odd-mass targets with large nonzero  $\mathcal{J}$ . We thus conclude that asserting the presence of NCNF solely based on observed deviation of  $A_{\text{exp}}$  from SSPM predictions may not be justified. Experimentally obtained  $\sigma_{\text{fis}}$  were reproduced by PACE3 in most cases, with  $a = \frac{A}{10}$ ,  $\frac{a_t}{a_n} = 1.00$ , and  $k_f = 1.00$  and without including shell effects in the calculation. However, the SM calculation with VECSTAT, in which the shell effect in the level density parameter and shell correction in the fission barrier were included, yielded lower  $\sigma_{\text{fis}}$  than those obtained experimentally for all reactions barring  $^{28}\text{Si} + ^{181}\text{Ta}$  and  $^{28}\text{Si} + ^{182}\text{W}$ . Observation of experimental  $\sigma_{\text{fis}}$  being larger than calculated  $\sigma_{\text{fis}}$  signifies the presence of NCNF in a given system. Thus all the reactions except  $^{28}\text{Si} + ^{181}\text{Ta}$  and  $^{28}\text{Si} + ^{182}\text{W}$  show clear signatures of NCNF in the present analysis. However, the dependence of this conclusion on a specific model and input parameters should be investigated further. Also, the outcome of fusion reactions in which signatures of NCNF are observed ought to be better described by a dynamical model.

## ACKNOWLEDGMENTS

The authors thank the Pelletron staff of IUAC for excellent support throughout the experiment, Mr. Abhilash S.R. for assistance in fabricating thin isotopic targets, and Mr. T. Varughese and Mr. P. Barua for maintaining the experimental facility. One of the authors (T.B.) acknowledges useful discussions with Ms. A. Parihari and financial support from the University Grants Commission (UGC), Government of India.

- 
- [1] B. Borderie, M. Berlinger, D. Gardés, F. Hanappe, L. Nowicki, J. Péter, B. Tamain, S. Agarwal, J. Girard, C. Gégouire, J. Matuszek, and C. Ngô, *Z. Phys. A* **299**, 263 (1981).
  - [2] J. Töke, R. Bock, G. X. Dai, A. Gobbi, S. Gralla, K. D. Hildenbrand, J. Kuzminski, W. F. J. Müller, A. Olmi, H. Stelzer, B. B. Back, and S. Bjørnholm, *Nucl. Phys. A* **440**, 327 (1985).
  - [3] V. S. Ramamurthy and S. S. Kapoor, *Phys. Rev. Lett.* **54**, 178 (1985).
  - [4] C.-C. Sahn, H.-G. Clerc, K.-H. Schmidt, W. Reisdorf, P. Armbruster, F. P. Heßberger, J. G. Keller, G. Münzenberg, and D. Vermeulen, *Nucl. Phys. A* **441**, 316 (1985).
  - [5] A. C. Berriman, D. J. Hinde, M. Dasgupta, C. R. Morton, R. D. Butt, and J. O. Newton, *Nature (London)* **413**, 144 (2001).
  - [6] D. J. Hinde, M. Dasgupta, and A. Mukherjee, *Phys. Rev. Lett.* **89**, 282701 (2002).
  - [7] R. Rafiei, R. G. Thomas, D. J. Hinde, M. Dasgupta, C. R. Morton, L. R. Gasques, M. L. Brown, and M. D. Rodriguez, *Phys. Rev. C* **77**, 024606 (2008).
  - [8] E. Prasad, K. M. Varier, R. G. Thomas, P. Sugathan, A. Jhingan, N. Madhavan, B. R. S. Babu, Rohit Sandal, Sunil Kalkal, S. Appannababu, J. Gehlot, K. S. Golda, S. Nath, A. M. Vinodkumar, B. P. Ajith Kumar, B. V. John, Gayatri Mohanto, M. M. Musthafa, R. Singh, A. K. Sinha, and S. Kailas, *Phys. Rev. C* **81**, 054608 (2010).
  - [9] A. Shamlath, M. Shareef, E. Prasad, P. Sugathan, R. G. Thomas, A. Jhingan, S. Appannababu, A. K. Nasirov, A. M. Vinodkumar, K. M. Varier, C. Yadav, B. R. S. Babu, S. Nath, G. Mohanto,

- Ish Mukul, D. Singh, and S. Kailas, *Nucl. Phys. A* **945**, 67 (2016).
- [10] B. B. Back, R. R. Betts, J. E. Gindler, B. D. Wilkins, S. Saini, M. B. Tsang, C. K. Gelbke, W. G. Lynch, M. A. McMahan, and P. A. Baisden, *Phys. Rev. C* **32**, 195 (1985).
- [11] R. Tripathi, K. Sudarshan, S. Sodaye, S. K. Sharma, and A. V. R. Reddy, *Phys. Rev. C* **75**, 024609 (2007).
- [12] R. du Rietz, E. Williams, D. J. Hinde, M. Dasgupta, M. Evers, C. J. Lin, D. H. Luong, C. Simenel, and A. Wakhle, *Phys. Rev. C* **88**, 054618 (2013).
- [13] Tathagata Banerjee, S. Nath, and Santanu Pal, *Phys. Rev. C* **91**, 034619 (2015).
- [14] Tapan Rajbongshi, Neeraj Kumar, S. R. Abhilash, D. Kabiraj, and K. Kalita, Proc. DAE Symp. Nucl. Phys. **59**, 864 (2014).
- [15] Tathagata Banerjee, P. V. Laveen, M. Shareef, S. R. Abhilash, J. Gehlot, S. Ojha, and D. Kabiraj, Proc. DAE Symp. Nucl. Phys. **59**, 948 (2014).
- [16] Tathagata Banerjee, S. R. Abhilash, S. Ojha, and D. Kabiraj, Proc. DAE Symp. Nucl. Phys. **60**, 982 (2015).
- [17] S. R. Abhilash, J. Gehlot, Tathagata Banerjee, K. Selvakumar, Jasmeet Kaur, and D. Kabiraj, *J. Radioanal. Nucl. Chem.* **305**, 749 (2015).
- [18] A. Jhingan, Gurpreet Kaur, N. Saneesh, T. Banerjee, R. Ahuja, B. R. Behera, and P. Sugathan, Proc. DAE Symp. Nucl. Phys. **59**, 830 (2014).
- [19] A. Jhingan, P. Sugathan, Gurpreet Kaur, K. Kapoor, N. Saneesh, T. Banerjee, H. Singh, A. Kumar, B. R. Behera, and B. K. Nayak, *Nucl. Instrum. Methods A* **786**, 51 (2015).
- [20] E. T. Subramanium, B. P. Ajith Kumar, and R. K. Bhowmik, software CANDLE: Collection and Analysis of Nuclear Data using Linux nEtworK (unpublished).
- [21] V. E. Viola, K. Kwiatkowski, and M. Walker, *Phys. Rev. C* **31**, 1550 (1985).
- [22] R. Vandenbosch and J. R. Huizenga, *Nuclear Fission* (Academic, New York, 1973).
- [23] R. D. Butt, M. Dasgupta, I. Gontchar, D. J. Hinde, A. Mukherjee, A. C. Berriman, C. R. Morton, J. O. Newton, E. Stuchbery, and J. P. Lestone, *Phys. Rev. C* **65**, 044606 (2002).
- [24] R. D. Butt, D. J. Hinde, M. Dasgupta, A. C. Berriman, A. Mukherjee, C. R. Morton, and J. O. Newton, *Phys. Rev. C* **66**, 044601 (2002).
- [25] N. Tajima, *Phys. Rev. C* **91**, 014320 (2015).
- [26] I. Halpern and V. M. Strutinsky, in *Proceedings of the Second United Nations International Conference on the Peaceful Uses of Atomic Energy, Geneva, 1958* (United Nations, New York, 1958), Vol. 15, p. 408.
- [27] A. J. Sierk, *Phys. Rev. C* **33**, 2039 (1986).
- [28] M. G. Itkis and A. Ya. Rusanov, *Phys. Part. Nuclei* **29**, 160 (1998).
- [29] K. Hagino, N. Rowley, and A. T. Kruppa, *Comput. Phys. Commun.* **123**, 143 (1999).
- [30] A. Gavron, *Phys. Rev. C* **21**, 230 (1980).
- [31] R. H. Spear, *Phys. Rep.* **73**, 369 (1981).
- [32] P. Moller, J. R. Nix, W. D. Myers, and W. J. Swiatecki, *At. Data Nucl. Data Tables* **59**, 185 (1995).
- [33] <http://www.nndc.bnl.gov/>.
- [34] R. Tripathi, K. Sudarshan, S. K. Sharma, K. Ramachandran, A. V. R. Reddy, P. K. Pujari, and A. Goswami, *Phys. Rev. C* **79**, 064607 (2009).
- [35] D. J. Hinde, C. R. Morton, M. Dasgupta, J. R. Leigh, J. C. Mein, and H. Timmers, *Nucl. Phys. A* **592**, 271 (1995).
- [36] Lagy T. Baby, Vandana Tripathi, J. J. Das, P. Sugathan, N. Madhavan, A. K. Sinha, M. C. Radhakrishna, P. V. Madhusudhana Rao, S. K. Hui, and K. Hagino, *Phys. Rev. C* **62**, 014603 (2000).
- [37] J. Sadhukhan, Ph.D. Thesis, Homi Bhabha National Institute, 2012 (unpublished).
- [38] P. Fröbrich and I. I. Gontchar, *Phys. Rep.* **292**, 131 (1998).
- [39] N. Bohr and J. A. Wheeler, *Phys. Rev.* **56**, 426 (1939).
- [40] V. M. Strutinsky, *Phys. Lett. B* **47**, 121 (1973).
- [41] K. Mahata, S. Kailas, and S. S. Kapoor, *Phys. Rev. C* **92**, 034602 (2015).
- [42] W. D. Myers and W. J. Swiatecki, Lawrence Berkeley National Laboratory Report No. LBL-36803, 1994 (unpublished).
- [43] W. D. Myers and W. J. Swiatecki, *Nucl. Phys. A* **601**, 141 (1996).
- [44] A. V. Ignatyuk, M. G. Itkis, V. N. Okolovich, G. M. Smirenkin, and A. Tishin, *Yad. Fiz.* **21**, 485 (1975) [*Sov. J. Nucl. Phys.* **21**, 255 (1975)].
- [45] W. Reisdorf, *Z. Phys. A* **300**, 227 (1981).
- [46] K. Ramachandran, A. Chatterjee, A. Navin, K. Mahata, A. Shrivastava, V. Tripathi, S. Kailas, V. Nanal, R. G. Pillay, A. Saxena, R. G. Thomas, Suresh Kumar, and P. K. Sahu, *Phys. Rev. C* **73**, 064609 (2006).
- [47] D. J. Hinde, R. J. Charity, G. S. Foote, J. R. Leigh, J. O. Newton, S. Ogaza, and A. Chatterjee, *Nucl. Phys. A* **452**, 550 (1986).
- [48] J. P. Lestone, J. R. Leigh, J. O. Newton, D. J. Hinde, J. X. Wei, J. X. Chen, S. Elfstrom, and M. Zielinska-Pfabe, *Nucl. Phys. A* **559**, 277 (1993).
- [49] K. Mahata, S. Kailas, A. Shrivastava, A. Chatterjee, A. Navin, P. Singh, S. Santra, and B. S. Tomar, *Nucl. Phys. A* **720**, 209 (2003).
- [50] A. Saxena, D. Fabris, G. Prete, D. V. Shetty, G. Viesti, B. K. Nayak, D. C. Biswas, R. K. Choudhury, S. S. Kapoor, M. Lunardon, S. Moretto, G. Nebbia, S. Pesente, V. Rizzi, A. M. Samant, M. Barbui, E. Fioretto, M. Cinausero, A. Brondi, G. La Rana, R. Moro, E. Vardaci, N. Gelli, and F. Lucarelli, *Nucl. Phys. A* **730**, 299 (2004).
- [51] H. Ikezoe, N. Shikazono, Y. Nagame, Y. Sugiyama, Y. Tomita, K. Ideno, I. Nishinaka, B. J. Qi, H. J. Kim, A. Iwamoto, and T. Ohtsuki, *Phys. Rev. C* **46**, 1922 (1992).
- [52] A. L. Caraley, B. P. Henry, J. P. Lestone, and R. Vandenbosch, *Phys. Rev. C* **62**, 054612 (2000).
- [53] D. J. Hinde, M. Dasgupta, J. R. Leigh, J. P. Lestone, J. C. Mein, C. R. Morton, J. O. Newton, and H. Timmers, *Phys. Rev. Lett.* **74**, 1295 (1995).
- [54] V. M. Strutinsky, *Nucl. Phys.* **27**, 348 (1961).
- [55] J. P. Lestone, A. A. Sonzogni, M. P. Kelly, and R. Vandenbosch, *Phys. Rev. C* **56**, R2907(R) (1997).
- [56] B. K. Nayak, R. G. Thomas, R. K. Choudhury, A. Saxena, P. K. Sahu, S. S. Kapoor, R. Varma, and D. Umakanth, *Phys. Rev. C* **62**, 031601(R) (2000).
- [57] R. G. Thomas, B. K. Nayak, A. Saxena, D. C. Biswas, L. M. Pant, and R. K. Choudhury, *Phys. Rev. C* **65**, 057601 (2002).
- [58] D. J. Hinde, J. O. Newton, J. R. Leigh, and R. J. Charity, *Nucl. Phys. A* **398**, 308 (1983).
- [59] D. C. Biswas, Nishant Kumar, Shradha Dubey, G. K. Prajapati, B. N. Joshi, K. Mahata, Y. K. Gupta, S. Mukhopadhyay, L. S.

- Danu, S. Sodaye, R. P. Vind, and B. V. John, Proc. DAE Symp. Nucl. Phys. **60**, 568 (2015).
- [60] K. Nishio, H. Ikezoe, S. Mitsuoka, and J. Lu, *Phys. Rev. C* **62**, 014602 (2000).
- [61] E. Williams, D. J. Hinde, M. Dasgupta, R. du Rietz, I. P. Carter, M. Evers, D. H. Luong, S. D. McNeil, D. C. Rafferty, K. Ramachandran, and A. Wakhle, *Phys. Rev. C* **88**, 034611 (2013).
- [62] A. Chatterjee, A. Shrivastava, S. Kailas, A. Navin, P. Singh, S. K. Datta, T. Madhusoodhanan, S. Mandal, and M. K. Sharan, Proc. DAE Symp. Nucl. Phys. **39B**, 170 (1996).
- [63] B. R. Behera, S. Jena, M. Satpathy, S. Roy, P. Basu, M. K. Sharan, M. L. Chatterjee, S. Kailas, K. Mahata, and S. K. Datta, *Phys. Rev. C* **66**, 047602 (2002).
- [64] F. Videbaek, R. B. Goldstein, L. Grodzins, S. G. Steadman, T. A. Belote, and J. D. Garrett, *Phys. Rev. C* **15**, 954 (1977).
- [65] M. Oghihara, H. Fujiwara, S. C. Jeong, W. Galster, S. M. Lee, Y. Nagashima, T. Mikumo, H. Ikezoe, K. Ideno, Y. Sugiyama, and Y. Tomita, *Z. Phys. A* **335**, 203 (1990).
- [66] B. Qi, H. Ikezoe, Y. Sugiyama, Y. Tomita, K. Ideno, and H. J. Kim, JAERI Lab Report JAERI-M-91-188, November 1991 (unpublished).
- [67] D. J. Hinde, W. Pan, A. C. Berriman, R. D. Butt, M. Dasgupta, C. R. Morton, and J. O. Newton, *Phys. Rev. C* **62**, 024615 (2000).
- [68] B. B. Back, J. G. Keller, A. Worsham, B. G. Glagola, D. Henderson, S. Kaufman, S. J. Sanders, R. Siemssen, F. Videbaek, and B. D. Wilkins, Report No. CONF-860396-13, presented at the Symposium on the Many Facets of Heavy Ion Fusion Reactions, held at Argonne National Laboratory, March 24–26, 1986 (unpublished).
- [69] H. Q. Zhang, C. L. Zhang, C. J. Lin, Z. H. Liu, F. Yang, A. K. Nasirov, G. Mandaglio, M. Manganaro, and G. Giardina, *Phys. Rev. C* **81**, 034611 (2010).
- [70] L. G. Moretto, K. X. Jing, R. Gatti, G. J. Wozniak, and R. P. Schmitt, *Phys. Rev. Lett.* **75**, 4186 (1995).
- [71] R. N. Sagaidak, G. N. Kniajeva, I. M. Itkis, M. G. Itkis, N. A. Kondratiev, E. M. Kozulin, I. V. Pokrovsky, A. I. Svirikhin, V. M. Voskressensky, A. V. Yerebin, L. Corradi, A. Gadea, A. Latina, A. M. Stefanini, S. Szilner, M. Trotta, A. M. Vinodkumar, S. Beghini, G. Montagnoli, F. Scarlassara, D. Ackermann, F. Hanappe, N. Rowley, and L. Stuttgé, *Phys. Rev. C* **68**, 014603 (2003).
- [72] L. Corradi, B. R. Behera, E. Fioretto, A. Gadea, A. Latina, A. M. Stefanini, S. Szilner, M. Trotta, Y. Wu, S. Beghini, G. Montagnoli, F. Scarlassara, R. N. Sagaidak, S. N. Atutov, B. Mai, G. Stancari, L. Tomassetti, E. Mariotti, A. Khanbekyan, and S. Veronesi, *Phys. Rev. C* **71**, 014609 (2005).
- [73] R. N. Sagaidak and A. N. Andreyev, *Phys. Rev. C* **79**, 054613 (2009).
- [74] G. Mohanto, N. Madhavan, S. Nath, J. Gehlot, I. Mukul, A. Jhingan, T. Varughese, A. Roy, R. K. Bhowmik, I. Mazumdar, D. A. Gothe, P. B. Chavan, J. Sadhukhan, S. Pal, M. Kaur, V. Singh, A. K. Sinha, and V. S. Ramamurthy, *Phys. Rev. C* **88**, 034606 (2013).
- [75] C. Schmitt, K. Mazurek, and P. N. Nadtochy, *Phys. Lett. B* **737**, 289 (2014).